Heliyon 10 (2024) e35264

Contents lists available at ScienceDirect

Heliyon

journal homepage: www.cell.com/heliyon

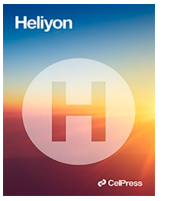

Research article

Silver/tannic acid nanoparticles/ poly-L-lysine decorated polyvinyl alcohol-hydrogel as a hybrid wound dressing

Fatemeh Hakimi [a], Hadi Balegh [b], Parham Sarmadi fard [b], Fahimeh Kazeminava [c], Sheyda Moradi [d], Mehdi Eskandari [e], Zainab Ahmadian [b,f,*]

[a] Department of Pharmaceutical Biomaterials, School of Pharmacy, Zanjan University of Medical Sciences, Zanjan, Iran
[b] Department of Pharmaceutics, School of Pharmacy, Ardabil University of Medical Sciences, Ardabil, Iran
[c] Drug Applied Research Center, Faculty of Medicine, Tabriz University of Medical Sciences, Tabriz, Iran
[d] Department of Chemistry, Faculty of Science, University of Mohaghegh Ardabili, Ardabil, Iran
[e] Department of Physiology, Faculty of Medicine, Zanjan University of Medical Sciences, Zanjan, Iran
[f] Department of Pharmaceutics, School of Pharmacy, Lorestan University of Medical Sciences, Korramabad, Iran

ARTICLE INFO

Keywords:
Anti-bacterial
Hybrid hydrogel
Polyvinyl alcohol
Hyperbranched poly L-lysine
Silver/ tannic acid nanoparticle
Wound healing

ABSTRACT

Hydrogels containing antimicrobial materials have emerged as attractive platforms for wound treatment in the past decade due to their favorable bio-mimicking properties, excellent modulation of bacterial infection, and ability to minimize bacterial resistance. Herein, a hybrid combination of polyvinyl alcohol (PVA), hyperbranched poly L-lysine (L), tannic acid decorated AgNPs (AgTA NPs), loaded with Allantoin (Alla) is used to fabricate PLAg-Alla hydrogel dressing via the freeze-thaw method without use of any chemical cross-linker. The PLAg-Alla hydrogel possesses a great structure, is biodegradable, and safe, and exhibits high antibacterial potential, all required for efficient wound healing. The incorporation of AgTA and poly L-lysine (L) within the hydrogel contributes to the enhancement of antibacterial ability, as well as effectively promoting the wound healing. This hybrid hydrogel possessed favorable physicochemical features, robust antibacterial properties, and accelerated wound healing *in vivo* as promising dressing for the clinical application.

1. Introduction

In recent years, wounds have been identified as a challenging issue that often leads to increased mortality rates. The main obstacle in the wound healing process is the risk of bacterial infections especially from *staphylococcus aureus* bacteria [1–3]. Bacteria can easily enter the body through the wound site and penetrate in deeper layers of the skin. This may potentially lead to sepsis, resulting in a significant risk of amputation and morbidity [4,5]. Therefore, an antibacterial wound dressing is required to inhibit infection and bacterial growth. Furthermore, an ideal wound dressing should possess the following characteristics: maintaining a moist wound environment, protecting the wound from infection, and being biocompatible [6]. Unfortunately, traditional dry dressings often fail to provide the necessary moisture and tend to adhere to the wound, resulting in tissue injury upon removal. However, common traditional wound dressing, such as gauze and bandages, play a crucial role in the initial stages of wound healing [7]. Hydrogels are considered promising materials for wound treatment, as they can be prepared from various polymers and offer versatility [8].

* Corresponding author. Ardabil University of Medical Sciences, Ardabil, Iran.
E-mail addresses: z.ahmadian@arums.ac.ir, zainabahmadian007@gmail.com (Z. Ahmadian).

https://doi.org/10.1016/j.heliyon.2024.e35264
Received 18 January 2024; Received in revised form 24 July 2024; Accepted 25 July 2024
Available online 26 July 2024

List of abbreviations

AgNPs	Silver nanoparticles
Alla	Allantoin
AgTA NPs	Tannic acid modified AgNPs
$AgNO_3$	Silver nitrate
DLS	Dynamic light scattering
DTA	Diffraction thermogravimetric analysis
FWHM	Full width at half maximum
IR	Infrared spectra
KOH	Potassium hydroxide
L	Hyper branched poly L-Lysine
PVA	Polyvinyl alcohol
PAg	PVA loaded with AgTA NPs
PLAg	PAg loaded with L
PLAg-Alla	PLAg loaded with Alla
THF	Tetrahydrofuran
XRD	X-ray diffraction

Hydrogels, being a polymeric network with physical or chemical cross-links, possess the unique ability to swell and absorb water [9]. They can create a biomimetic barrier against bacteria to protect the wound [10]. Additionally, hydrogels can mimic the natural extracellular matrix which not only reduces pain but also accelerates epidermal regeneration [11]. Developing new hydrogel dressing with low toxicity, cost-effectiveness, simple preparation processes and antimicrobial potential is considered an ideal platform for wound treatment. Recently, hybrid hydrogels with multifunctional potential have been investigated for effective wound treatment [12,13]. In this study, a hybrid hydrogel dressing was reasonably fabricated by simply mixing PVA, AgTA NPs, and hyperbranched poly L-lysin [14–17]. PVA is a water-soluble polymer that is widely used in medicine for various applications, such as tissue engineering and drug delivery systems. However, due to the lack of antibacterial properties in pure PVA, researchers often prepare PVA-based antibacterial hydrogels by incorporating metal nanoparticles or other agents [18]. Additionally, studies have demonstrated the high antimicrobial efficiency of AgNPs in wound treatment, yet their clinical use remains controversial due to potential toxicity concerns. AgNPs can be further modified with natural antimicrobial agents to address these concerns [19–21]. In this context, TA, a natural polyphenol, is used to develop antibacterial materials through the green synthesis of biocompatible AgNPs. TA can form multiple hydrogen bonds with different polymers (e.g., PVA, chitosan, agarose) enabling the fabrication of versatile hydrogels. This makes TA a valuable component in advanced multifunctional wound dressings, offering a non-antibiotic treatment approach [22–25]. Furthermore, poly lysine, a natural antimicrobial peptide, with strong antibacterial characteristics, is edible, biodegradable, non-toxic, and can be produced at a low cost. It has been used as an antimicrobial food additive and has found applications in gene delivery, tissue engineering, wound repair, and other biomedical fields [26,27]. Additionally, allantoin (Alla) was used as a drug model in this study. Alla, a nature-based drug, is clinically used to manage acne, scars, eczema, and wounds and has showed antioxidant, anti-inflammatory and cell proliferating potentials [25,28–30]. Therefore, the aim of this study is to design an Alla-loaded hybrid hydrogel that has antibacterial and wound healing properties and is biocompatible at the same time.

2. Method and materials

2.1. Materials

All of the chemical materials and drugs, including PVA, TA, Silver nitrate ($AgNO_3$), L-lysine hydrochloride, Disodium hydrogen phosphate, Sodium dihydrogen phosphate, Phosphoric acid, Methanol, Potassium hydroxide (KOH), Tetrahydrofuran (THF), Sodium citrate, Petroleum ether, Ketamine, Xylazine and Alla were purchased from (Sigma-Aldrich, USA) and (Sigma-Aldrich, Germany) with analytical grade. Bacterial cells were prepared from the Pasteur Institute (Iran). The Ethics Committee of Ardabil University of Medical Sciences approved this study with the ethics code IR.ARUMS.AEC.1401.020, ensuring it adhered to the institutional and international guidelines for animal care.

2.2. Preparation and characterization

2.2.1. Preparation of AgTA NPs, hyperbranched poly L-lysine and PVA based hydrogel

To fabricate the PLAg-Alla hydrogel, AgTA NPs, hyperbranched poly L-lysine (L) and Alla were incorporated into a PVA solution using a single cycle of freeze-thaw. Initially, AgTA NPs and hyperbranched poly L-lysine were synthesized. Next, the optimal concentration of AgTA NPs was determined and PVA-based hydrogel was prepared with optimized ratio of the AgTA NPs. To synthesize AgTA NPs via green synthesis method, an aqueous solution containing $AgNO_3$ (0.017 % W/V) was heated to its boiling point and refluxed with continuous stirring. Subsequently, an aqueous solution of sodium citrate (4 % W/V) and TA (5 % W/V) was introduced

into the silver nitrate solution under stirring. The immediate transformation of the solution to a yellow color indicated the successful formation of AgTA NPs. The resulting solution was stirred vigorously for 15 min and then allowed to cool at room temperature. Next, the solution containing AgTA NPs was centrifuged at 12,000 rpm for 15 min and the supernatant was discarded. The precipitate was collected as AgTA NPs. Hyperbranched poly L-lysine was prepared via the thermal polymerization of L-lysine-hydrochloride according to a previous study [31]. This process results in the formation of multi-branched poly L-lysin. In summary, we completely mixed L-lysine hydrochloride and KOH to form a consistent paste. We kept the mixture at 150 °C for 48 h after adding paraffin oil. Next, we discarded the paraffin oil and washed the residue mixture three times with ether. The obtained brown solid product was then dissolved in methanol, and the side products were removed by filtration. Finally, tetrahydrofuran (THF) was added to the filtered solution, and a yellow-brown precipitate was obtained, which is the Poly L-lysine. In this study, 4 types of hydrogels including, PVA alone, PAg (PVA based hydrogel contain AgTA NPs), PLAg (PVA based hydrogel contain AgTA NP and L), and PLAg-Alla (PVA based hydrogel contain AgTA NPs, L and Alla) were prepared via the freeze-thaw method. In all hydrogels, the concentrations of PVA, L, and Alla were 10 %, 1 %, and 1 % W/V, respectively. To optimize hydrogel preparation, we fabricated a series of PAg hydrogels with decreasing concentrations of 0.1, 0.05, and 0.01 wt% of AgTA NPs. Based on the results of characterizing PAg hydrogels, including, initial water content, water retention, swelling and degradation, the PAg hydrogel with AgTA NPs 0.01 wt% was investigated for loading hyperbranched poly L-lysin and Alla. To prepare the hydrogels, a 10 % W/V solution of PVA was prepared in deionized water and then an aqueous solution of AgTA NPs (0.01 % W/V) was added to PVA solution. To form PAg hydrogel, a freeze-thaw cycle was performed (at −25° (18 h) and at room temperature (6 h)). Notably, to prepare PLAg and PLAg- Alla hydrogels, poly L-lysin and Alla were added to the mixture of PAg before the freeze-thaw cycle to prepare hydrogels containing these materials. The AgTA NPs, PAg, PLAg and PLAg- Alla hydrogels were characterized by DLS, FTIR, XRD, TGA, antibacterial assay, and *in vivo* wound healing examinations.

2.2.2. Instrumental analysis

The samples were analyzed to confirm the hydrogel formation and drug loading using Infrared spectroscopy (IR). An IR spectrometer (Bruker, Germany) was utilized, and ATR-FTIR spectra were recorded in the wavenumber range of 400–4000 cm^{-1} at room temperature. X-ray diffraction (XRD, Philips PW1730) analysis was performed to study the crystallinity of the raw material and the product at room temperature, with a 2θ range of 10–80°θ. The thermal degradation of the samples was investigated via thermogravimetric analysis (TGA, STA6000). The thermal behavior study was conducted with a heating temperature range of 25–800 °C and a heating rate of 10 °C min^{-1} under a nitrogen atmosphere. The size and charge of AgTA NPs were determined using dynamic light scattering (DLS, ZN Series).

2.2.3. The initial water content measurement

For this test, the fresh-fabricate hydrogels were weighed and their weight recorded. Next, samples were dried in an oven at 60 °C and weighed again. The initial water content was calculated using formula [1], where W_0 and W_d representing the initial weight and the weight of the dried hydrogel [32].

$$\textit{Initial water content}\ (\%) = \frac{W0 - Wd}{W0} \times 100 \tag{1}$$

2.2.4. The water retention capacity measurement

To perform this test, the weighed pieces of each hydrogel after preparation were placed in PBS (pH 7.4) for 48 h at 37 °C to swell. After this time, the hydrogels were taken out from the PBS and left at room temperature. At specific times, the hydrogels were weighed. After the last time of test, the hydrogels were placed in the oven to dry completely and then weighed again. The water retention percentage for each hydrogel was obtained using the following formula [2]: In the formula below, M_t is the weight of the hydrogel at time t and M_0 is the weight of the dried hydrogel after oven drying [33].

$$\textit{Water retention capacity}\ (\%) = \frac{(Mt - M0)}{M0} \times 100 \tag{2}$$

2.2.5. Swelling measurement

A swelling test evaluated the ability of different samples to absorb water. First, pieces of dried hydrogel were weighed before swelling (W_0). Next, the weighed hydrogels were immersed in a PBS medium (pH 7.4) and kept at 37 °C. At specific time intervals, the swollen samples were taken out of the PBS solution, and the surface moist of hydrogel was removed with filter paper and weighed immediately (W_s). The weighed hydrogels were then re-incubated in PBS to assess swelling at different times. The swelling percentage at any time was calculated using the following equation [3,34].

$$\textit{Swelling}\ (\%) = \frac{(Ws - W0)}{W0} \times 100 \tag{3}$$

2.2.6. The degradation measurement

To evaluate the degradability of hydrogels, the initial weight (W0) of the samples was recorded. Next, the hydrogels were immersed in PBS (pH 7.4) and incubated at 37 °C. At distinct time intervals, the hydrogels were removed from the PBS and dried in an oven at 60 °C. The weight of the hydrogel samples after drying was determined (Wf) and the degradability percentage was calculated using equation [4,35].

$$Degradation\ (\%) = \frac{(W0 - Wf)}{W0} \times 100 \quad (4)$$

2.3. Antibacterial experiment

The antibacterial study of PVA hydrogels was conducted against gram-positive bacteria *Staphylococcus aureus* (ATCC ® 25,923™), and gram-negative bacteria *Escherichia coli* (ATCC ® 25,922™) using the plate counts assay [36]. A weighed amount of hydrogel was mixed with 1 mL of the bacterial suspension, which had a concentration of 10^6 CFU/mL and was diluted using 0.9 % normal saline. The mixture was incubated at room temperature for 24 h. After 24 h, the samples were diluted with PBS. Then, 100 μL of the resulting dilutions were cultured on Mueller Hinton agar medium and incubated at 37 °C for another 24 h. After the incubation time, the number of bacterial colonies was observed and counted. In this experiment, 20 mL of PBS was incubated with 1 mL of bacterial suspension in the same condition, as a negative control.

2.4. Wound healing screen

This test aimed to evaluate the effects of the prepared hydrogel on the wound healing process. The experiment involved Sprague-Dawley model rats that were randomly divided into four groups, each treated with Tegaderm™ film, PAg, PLAg, and PLAg-Alla. The animals were first anesthetized (ketamine, 50 mg mL^{-1} and xylazine, 20 mg mL^{-1}, intraperitoneal injection), their hair was shaved, and then a full-thickness wound (1 cm) was inducted on the dorsal region of the rats. Next, the wounds were covered with PVA based hydrogels and film. The wounds were screened and photographed on days 0, 3, 7, and 14. The photographs were analyzed using ImageJ software. Additionally, the wound size of each animal was calculated at time points of 0, 3, 7, and 14 days by following the equation. The percentage of remaining wound area was calculated using wound areas at time points (0) and (t) by following equation [5].

$$Wound\ area\ (\%) = \frac{(Wound\ area\ (t))}{(Wound\ area\ (0))} \times 100 \quad (5)$$

2.5. In vivo biocompatibility and histological studies

Animal toxicity of PLAg-Alla hydrogel against control group was investigated through the assessment of hematological and biochemical factors. In this context, 2 mL of blood was taken from each animal 14 days post treatment. 1 mL of the blood was placed in heparinized tubes to evaluate hematological factors and 1 mL was poured into non-heparinized tubes to assess biochemical factors. After killing the animals on the 14th day, a histological examination was performed for important tissues including the liver, kidney, and spleen. These tissues were first fixed in 4 % paraformaldehyde, then dehydrated and embedded in melted paraffin. Next, the tissues were cut into thin slices and stained with hematoxylin and eosin (H&E). Light microscopy evaluated the morphological changes in the tissue slices. Additionally, for the histological investigation of wound healing, the animal skin of different groups was removed to evaluate wound healing.

2.6. Statistical analysis

Statistical analysis was conducted to assess the significance of the experimental results. At least three independent replications for each dataset of all experiments were performed. The results are presented as mean ± SD (standard deviation). GraphPad Prism and Origin Pro software were utilized for statistical analysis, employing ANOVA. A difference (P) of less than 0.05 was considered significant between the hydrogel group and the control group.

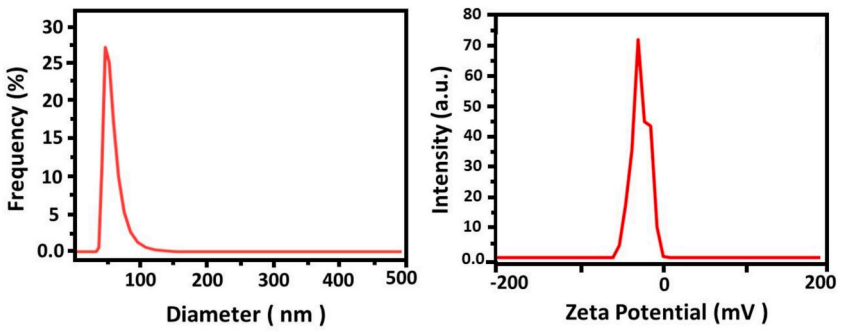

Fig. 1. Size and zeta potential curves of AgTA NPs.

3. Results and discussion

3.1. Ag/TA NPs particle size and zeta potential

The size and zeta potential of synthesized AgTA NPs were measured by dynamic light scattering (DLS), and the results are shown in Fig. 1. As seen in the diagram, the most dispersed particle size ranges between 35 and 65 nm, with approximately 27 % of AgTA NPs being 50 nm. Similarly, the zeta potential value for AgTA NPs is −25mV, indicating the stability and negative electrostatic charge of synthesized AgTA NPs in the solution phase. Additionally, the crystalline size of AgTA NPs was estimated using the Scherrer following equation [6]. Where, D, K, λ, β and θ parameters indicate size (nm), the Scherrer constant (0.9), the wavelength of X-ray source (0.154 nm), FWHM and peak position, respectively [37,38]. The parameters of Full width at half maximum (FWHM) and peak position were calculated from the XRD pattern of the AgTA NPs.

$$D\,(nm) = \frac{k\lambda}{\beta \cos\theta} \times 100 \tag{6}$$

The crystalline size for AgTA NPs was obtained to be 39 nm. The sizes obtained from both the DLS and Scherrer analyses for AgTA NPs were consistent with references [39,40]. The biological activity of AgNPs can be influenced by particle size, surface charge, and the reducing compound type used in their preparation process. The surface charge and hydrophilicity of stabilized TA on AgTA NPs play a crucial role in their stability and the interaction of NPs with bacterial cells, enhancing bactericidal activity. Furthermore, it was found that smaller particles of AgTA NPs can effectively promote the biological properties [40,41].

3.2. Hydrogel optimization

3.2.1. Initial water content of the hydrogel

Fig. 2 displays the results of the investigation into the initial water content of PVA hydrogels. The initial water content of PVA alone, PAg-0.1 (PAg hydrogel contain AgTA NPs 0.1 wt%), PAg-0.05 (PAg hydrogel contain AgTA NPs 0.05 wt%), and PAg-0.01(PAg hydrogel contain AgTA NPs 0.01 wt%) hydrogels was obtained in the range of 88–90 %. Additionally, the initial water content of hydrogels containing AgTA NPs was compared with that of PVA hydrogel. The results showed that the initial water content of PAg hydrogels did not show a statistically significant difference compared to each other, but they were higher compared to PVA alone. These findings indicate that the presence of Ag/TA in the structure of PVA hydrogel changes the amount of the initial water that is in the hydrogel. However, there is no significant difference in the effect of tested concentrations of AgTA NPs on the initial water content of the PVA hydrogel.

3.2.2. Water retention of PAg hydrogel

The water retention ability of PAg hydrogels was investigated in PBS (pH 7.4) at different time intervals (Fig. 3). As seen in the graph, the percentage of water retention in all of the hydrogels during the first 0.5 h of the test is about 700–750, with no significant difference between the three hydrogels at this time. During the first 2 h, the water retention capacity of PAg hydrogels is in the ranges from 300 to 440 %. The results show that over time, the water content and the amount of weight loss in PAg hydrogels decrease with a uniform slope, and the water retention capacity of PAg-0.1 hydrogel is higher compared to other samples. Furthermore, each hydrogel released over 90 % of its absorbed water within 8 h, following which the hydrogels' weight loss slope stayed nearly constant. The results of this test indicated that PAg hydrogels have almost the same ability to absorb and retain water, and the weight loss for all three hydrogels is one-third of the initial value after 4 h. As shown in Fig. 3, the PAg hydrogels rapidly absorbed water and gradually released it, suggesting their high hydrophilicity. This phenomenon can be explained by water molecules forming in the network structure of the

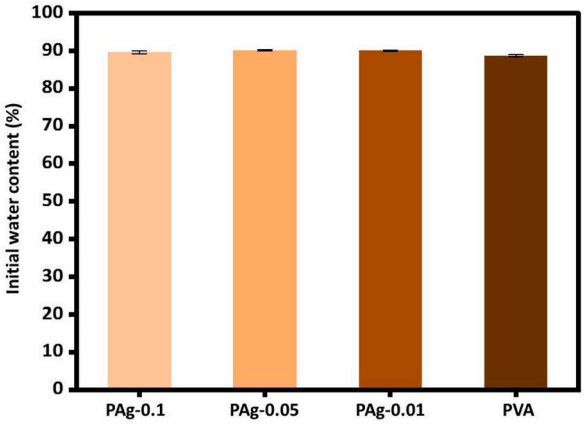

Fig. 2. Percentage of water content of PAg-0.1, PAg-0.05, PAg-0.01 and PVA hydrogels (n = 3; Mean ± SD).

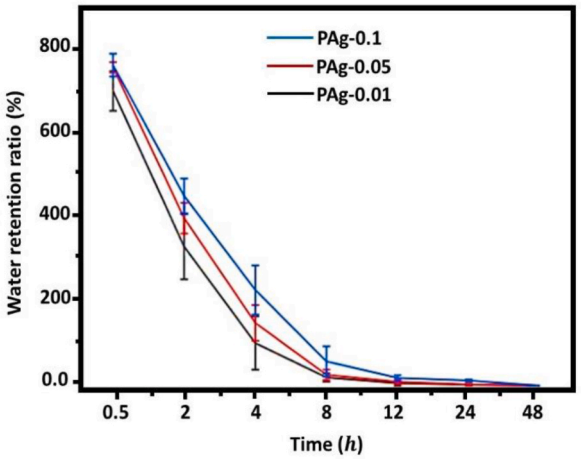

Fig. 3. Percentage of water retention of PAg-0.1, PAg-0.05 and PAg-0.01 hydrogels (n = 3; Mean ± SD).

hydrogel, which are classified into three groups: free or bulk water, intermediated water, and bound water. The initial loss of water retention within hydrogels can be related to the rapid evaporation of free water from the hydrogel sample [42].

3.2.3. *Swelling of PAg hydrogel*

The swelling properties of PVA and PAg hydrogels in PBS medium (pH 7.4) and up to 24 h are shown in Fig. 4. Also, the highest amount of water absorption and swelling among the PAg hydrogels is observed in the PAg-0.05 hydrogel. Fig. 4 shows that the % swelling of PVA hydrogels at all investigated concentrations was affected by the presence of AgTA NPs. This result may be related to hydrogen bonding between the hydroxyl groups of PVA and the synthesized AgTA NPs. In addition to the effect of functional groups on the swelling rate, the electrostatic repulsion and ionic fluctuations also influenced the swelling rate of PAg hydrogels. Furthermore, the rate of PAg swelling can be directly attributed to the number of active interactions in the hydrogel network. Additionally, the abundance of hydrophilic groups in the PAg hydrogel and the higher osmolality within the hydrogel network compared to the surrounding medium result in the uptake of water molecules and swelling of hydrogel structure. Previous studies have demonstrated similar results [43,44].

3.2.4. *Degradation of PAg hydrogel*

The degradation behavior of PVA and, PAg hydrogels in PBS (pH 7.4) and up to 48 h is shown in Fig. 5. As seen in the degradation curves, the prepared hydrogels have shown different degradation percentages. After 48 h, the amount of degradation for all hydrogels is almost similar, with about 13 % of the samples were degraded during this time. Similarly, the results show that during the first 8 h of the test, the samples have a higher degradation rate, with degradability ranging from 8 to 10 %. A comparison of their degradation results shows that there is no significant difference between the degradation behaviors of the prepared hydrogels.

As mentioned earlier, to optimize the hydrogel, a series of hydrogels were first fabricated by adding solutions of AgTA NPs with different concentrations to a PVA solution. The initial water content, water retention, swelling, and degradability properties of the

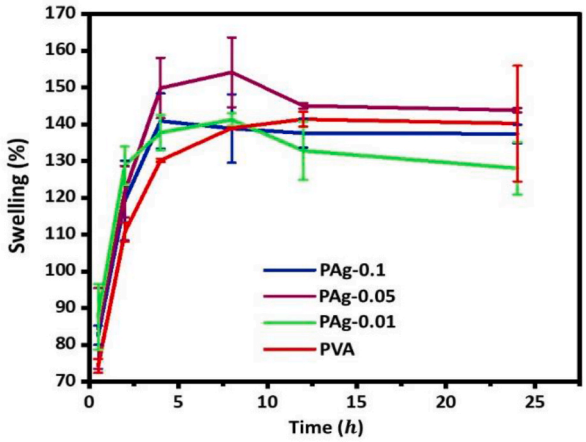

Fig. 4. Swelling of PVA, PAg-0.1, PAg-0.05 and PAg-0.01 hydrogels (n = 3; Mean ± SD).

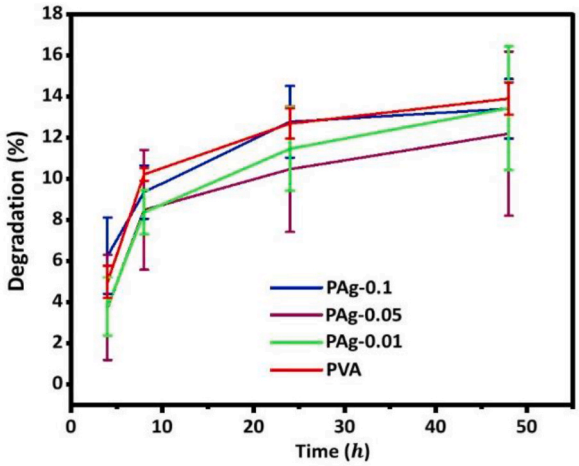

Fig. 5. Degradation of PVA, PAg-0.1, PAg-0.05 and PAg-0.01 hydrogels (n = 3; Mean ± SD).

hydrogels were then studied. The findings showed that changing the concentration of AgTA NPs did not affect these properties of the hydrogel. In this study, the initial water content and water retention ability were not significantly affected by the concentration of AgTA NPs. Similarly, the swelling and degradability tests indicated that various concentrations of AgTA NPs had no effect. Therefore, the lowest concentration of AgTA NPs was chosen for the preparation of the hydrogel due to its enhanced biosafety. Water absorption capacity and swelling are the important characteristics of hydrogels that affect their behavior, including the rate of therapeutics release and the absorbtion of wound secretions [45]. PVA is one of the most common synthetic polymers, widely used in biomedicine due to its high biocompatibility. However, PVA hydrogels have poor elastic properties, stiffness, and low hydrophilicity, which limits their use as a polymeric material in wound dressings [46]. As seen in the results, the multicomponent PVA hydrogel had shown a fast and high water absorption potential initially, likely due to the porous structure of the hydrogel. The degradation results showed that the PVA hydrogels had a low percentage of degradation. It seems that physical interactions of PVA with AgTA NPs and L (poly L-lysin) improved the stability of the hydrogel.

3.3. Physicochemical characterization

3.3.1. FTIR analysis

FT-IR technique has been applied to evaluate the chemical binding of the prepared hydrogel [47]. The FT-IR spectra of raw materials, including PVA polymer, L, TA, Ag(NO_3) and AgTA NPs, PVA alone hydrogel, and PAg hydrogels are shown in Fig. 6. In the infrared spectrum of PVA, the peak in the absorption region of 3100–3600 cm^{-1} corresponds to the stretching vibration of the OH group. Also, the observed peaks in the range of 1740–1640 cm^{-1} are related to stretching vibrations of C=O and C–O bonds of PVA polymer [48]. In the spectrum obtained for Ag(NO_3), the absorption peak at 3440 cm^{-1} is related to the stretching vibration of the OH bond, and the peaks observed at 1632 cm^{-1} and 1383 cm^{-1} are related to the stretching vibration of the C=O bond and the bending

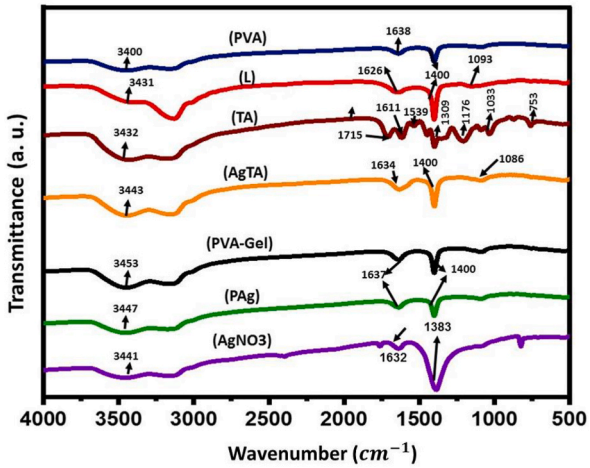

Fig. 6. FTIR of Ag(NO_3), TA, PVA, PVA-Gel, AgTA, poly L-lysin (L) and PAg.

vibration, respectively. In the spectrum obtained for TA, a broad peak at 3383 cm^{-1} and other peaks at 11,715, 1611, 1539, 1309, 1444, 1176, 1033 and 753 cm^{-1} are seen. These absorption bands are related to the stretching vibrations of phenolic OH and C–O bonds and the stretching vibration of C=O and C–O bonds. As seen in the FT-IR spectrum, PAg hydrogel shows all the characteristic peaks of the pure polymer and AgTA NPs. The peak at 1383 cm^{-1} of AgTA NPs in PAg hydrogel was shifted to a wavelength of 1400 cm^{-1} [49]. In the case of AgTA NPs, the peaks of 1033 cm^{-1} and 1176 cm^{-1} were combined, creating a broad peak at 1086 cm^{-1}. Also, the peaks of 1539 cm^{-1}, 1611 cm^{-1}, and 1715 cm^{-1} of TA were combined in AgTA, creating a peak at 1634 cm^{-1} [50]. FT-IR findings showed that AgTA NPs, and PAg hydrogels were formed correctly and the changes in the absorption spectra indicated the successful formation of the hydrogel with AgTA nanoparticles.

3.3.2. XRD spectroscopy

The XRD pattern of raw materials, AgTA and prepared hydrogels is shown in Fig. 7. Diffraction peaks of Ag salt at values of 37, 44, 64, and 77 °θ corresponding to crystal phases (111), (200), (220) and (311) have appeared (JCPDS No.O4–O783). Also, all of the diffraction peaks of Ag salt with less intensity are observed in XRD of AgTA [51]. In addition, the XRD pattern of Alla and poly L-lysin (L) confirm the presence of diffraction peaks related to their crystal phases at different values of 2θ. Similarly, the XRD of PVA shows a broad diffraction peak in the 2θ range of 18–22°, which is slightly shifted to higher 2θ values in PAg and PLAg hydrogel. Some of the peaks of raw materials and drugs are not observed in the PLAg-Alla hydrogel. These findings showed that some of the characteristic diffraction peaks of the raw materials were weakened or disappeared in the final hydrogel. These changes can be attributed to the successful presence of AgTA into the hydrogel structure, and the X-ray diffraction test also confirms the successful formation of the final hydrogel.

3.3.3. TGA analysis

The thermal stability of raw materials, nanoparticles, and prepared hydrogels was analyzed via TGA (Fig. 8). Thermal graphs for Ag (NO_3) and AgTA NPs revealed two main degradation peaks. Ag (NO_3) had a weight loss of 3.5 % at temperatures below 100 °C and 25 % at 350–550 °C. The graph for AgTA NPs indicated a weight loss of 7.5 % at 100 °C and 3.7 % at 100–600 °C. Ag (NO_3) and AgTA NPs had a total weight loss of 28 % and 11 %, respectively, up to 600 °C, with 70–90 % of their structure preserved. The PVA polymer and PAg hydrogel showed three and four degradation peaks, with the main peak of degradation occurring above 200 °C with a weight loss of more than 70 %. The PLAg hydrogel exhibited greater thermal stability at temperatures below 300 °C and less structure destruction. Notably, the peak at 200–300 °C can be related to the weakening of the hydrogel network, and the weight loss peak above 300 °C indicates the final stage of hydrogel degradation. The PAg hydrogel experienced weight loss at temperatures below 100 °C (3 %) and between 100 and 200 °C (17 %). The highest weight loss for PAg (78 %) occurred between 200 and 600 °C. The thermal analysis showed high thermal stability of the PAg hydrogel, which was improved by AgTA NPs. The PLAg hydrogel showed two stages of weight loss, with 10 % loss at 300 °C and 73 % at 300–450 °C. The PLAg hydrogel demonstrated more thermal stability at temperatures below 300 °C, reducing hydrogel structure destruction. Alla also shows weight loss peaks, with over 95 % occurring after 700 °C. The PLAg-Alla hydrogel has a similar weight loss process. Alla has three main weight loss peaks, with over 95 % of weight loss occurring after 700 °C. The PLAg-Alla hydrogel showed a weight loss process similar to PLAg hydrogel, with less weight loss in the first and second stages. The results of TGA and DTG analysis showed an initial weight loss for raw materials and prepared hydrogels, likely due to the evaporation of absorbed water and other volatile substances. The graph for PVA and hydrogel showed a high degree of degradation above 200 °C with a weight loss of 71 %, and the highest weight of PVA degraded at this stage. The second peak was due to the destruction of the side and main chains of PVA. The comparison of thermal analysis results showed that AgTA NPs had very high thermal stability, and the hydrogel containing AgTA NPs had higher thermal stability than the pure polymer, with the presence of AgTA NPs improving the stability properties of PVA.

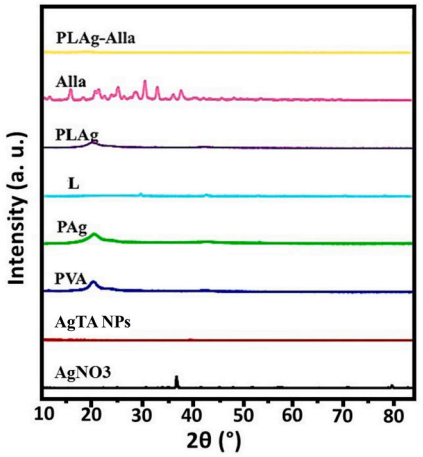

Fig. 7. Xrd of Ag(NO_3), AgTA NPs, PVA, L (poly L-lysine), PAg, PLAg, Alla, PLAg-Alla.

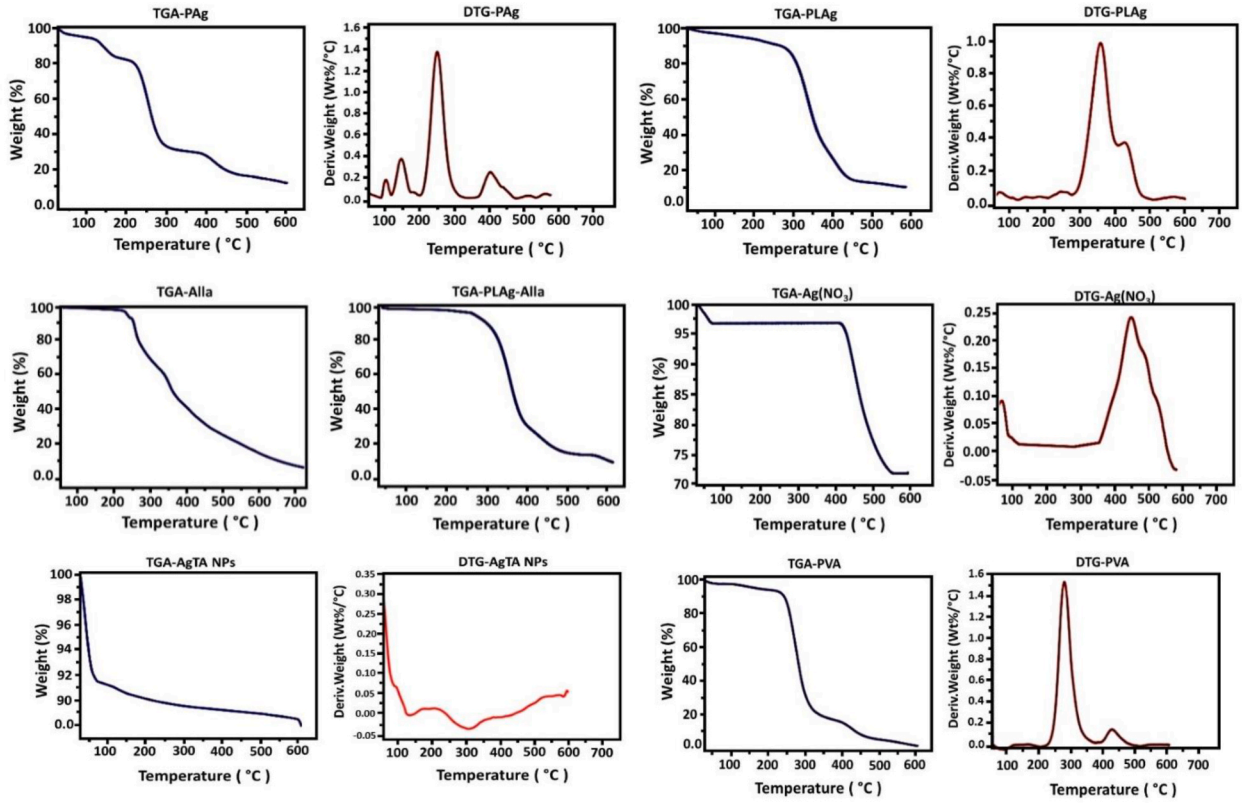

Fig. 8. TGA and DTG analysis of PVA polymer, $Ag(NO_3)$, AgTA NPs, PAg, PLAg, Alla and PLAg-Alla.

3.3.4. *The antibacterial activity of hydrogels*

The bacterial colony counting assay was used to investigate the antibacterial properties of AgTA NPs, PAg, PLAg, and PLAg-Alla hydrogels against *E coli* and *S. aureus* bacteria strains. As shown in Fig. 9, a large number of bacterial colonies were observed in the control groups after incubation for both bacteria strains. In contrast, no bacterial colonies are observed in the AgTA NPs solution and the prepared hydrogels, compared to the control groups. The results of the bacteria test show that the hydrogel and its components can inhibit the growth of microorganisms, demonstrating excellent antibacterial properties against gram-positive and gram-negative bacteria strains. This can be related to the inherent antibacterial properties of AgTA NPs, and poly L-lysin (L). AgNPs are antimicrobial

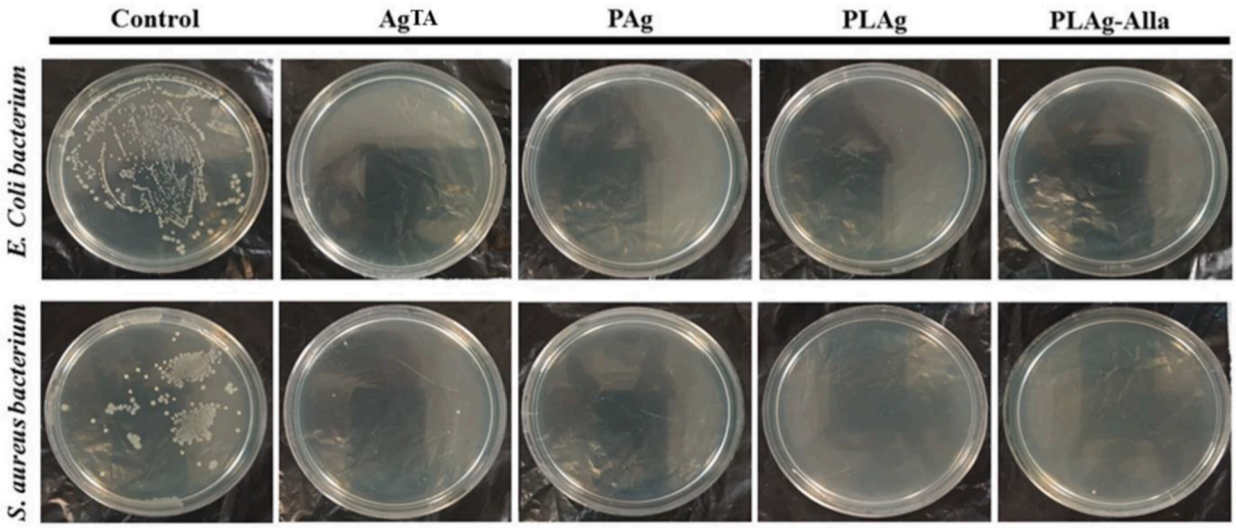

Fig. 9. Antibacterial efficacy of AgTA, PAg, PLAg, and PLAg-Alla by colony counting method.

compound that induces bactericidal effect through mechanisms, such as disruption of the bacteria cell membrane and cytoplasmic wall, ribosome denaturation and inhibition of protein synthesis [52]. Moreover, the presence of TA as an antimicrobial and reducing agent in the AgTA NPs result in the synergistic of bactericidal effect of Ag NPs. In addition to antibacterial ability of the AgTA NPs, the cationic nature of hyperbranched poly L-lysin that induces antibacterial effect via the electrostatic interaction with the negatively charged cell surfaces, resulting in bacteria cell death [53]. Similar results were observed with references [54–56]. In general, the antibacterial capacity of wound dressing hydrogels can promote more efficiency of their biological effect.

3.4. In vivo toxicity studies on PLAg-Alla hydrogel

3.4.1. Hematological and biochemical factors

The blood and biochemical factor values of the animals treated with PLAg-Alla hydrogel are shown in Fig. 10. Using the unpaired *t*-test, the average of each factor of the hydrogel group was compared with the control group (without treatment) and analyzed statistically. As seen in Fig. 10, the levels of blood factors of white blood cells (WBC), neutrophils (NEUT), lymphocytes (LYMPH), and monocytes (MONO) in animals treated with PLAg-Alla hydrogel show a statistically significant difference compared to the control group. Specifically, the levels of WBC, NEUT, and LYMPH showed a significant increase compared to the control group, while the number of MONOs significantly decreased compared to the control group. Additionally, the biochemical factors of alkaline phosphatase (ALP), albumin (Alb), calcium (Ca), phosphorus (PHO), creatine (KERA), and blood urea nitrogen (BUN) in the group treated with PLAg-Alla hydrogel showed no significant difference compared to the control group. Moreover, the levels of blood platelet factors (PLT), hematocrit (HCT), hemoglobin (HGB), and red blood cells (RBC) in treated animals are not significantly different from the control group. These findings showed that the levels of blood factors showed significant changes compared to the control group, likely due to the activation of the immune system and the triggering of inflammatory responses during the wound healing process. These results confirm the effect of the prepared hydrogel in the wound healing process as well as *in vivo* non-toxicity.

3.4.2. Histological study of kidney, liver, and spleen organs of animals

The histological changes in the kidney, liver, and spleen after the animal treatment with film, PAg, PLAg and PLAg-Alla hydrogels are shown in Fig. 11. As seen in the pictures, the hematoxylin-eosin (H&E) staining of these vital organs does not show any tissue damage such as necrotic tissue (dead tissue) or changes in the structure of the cells, in the hydrogel groups compared to the film group. Additionally, no morphological changes indicating proliferative changes related to blood cells, hemotoxicity, or inflammatory symptoms were observed in animals treated with hydrogel. In the images of kidney tissue samples, no signs of necrosis or tissue destruction can be seen. The shape of the glomeruli is completely normal, and the glomerular capillary rings do not show any signs of tissue death and congestion (hypertrophy). Furthermore, a histological examination of the spleen did not show signs of atrophy or hypertrophy. The ratio of white to red pulps in the spleen and the population of white pulps were normal. The histological results of kidney, liver, and spleen confirmed the prevention of cell damage in these organs in animals treated with hydrogels.

3.4.3. Evaluation of wound histological

H&E staining was performed on skin tissue sections to evaluate the wound histologically after 14 days of treatment (Fig. 12). The histological examination of the skin indicated that the wound surface was covered with new epithelial tissue in all groups. In the skin samples from the PLAg-Alla group, the formation of epidermal tissue and new buds was more organized, uniform, and regular. Additionally, a higher density of collagen fibers and fibroblasts was observed in the dermis of the PLAg-Alla group's skin samples. The presence of inflammatory cells and remnants of necrotic tissue was reduced in the PLAg-Alla group. Furthermore, scar tissue was not observed inthis group.

3.4.4. In vivo wound healing study

The wound site was screened during treatment, and the wound area was calculated using ImageJ software. The evaluation of the wound in each group is shown in Fig. 13A and B. The hydrogel-treated animals exhibited a faster healing process compared to the film group. The wound area on day 3 after surgery was significantly smaller for animals treated with PLAg-Alla than those treated with the film group, and it continued to decrease on days 7 and 14. The PLAg and PLAg-Alla treated animals presented a promoted wound closure rate, with approximately 98–99 % of the wound zone regenerating during the test period. These observations can be explained to the effects of hydrogels on the wound hydration, their swelling capacity to absorb wound exudates, and the effects of the loaded Alla in promoting cell proliferation. The high antimicrobial efficiency due to the presence of antimicrobial NPs also contributed to these results. This study concluded that PAg and PLAg-Alla hydrogel had a better regeneration rate and shrinkage compared to the other groups. These findings can be related to the combination and enhancement of the therapeutic properties of the hydrogel components, such as antibacterial, homeostasis, anti-inflammatory effects, and the induction of extracellular matrix formation within the hydrogel structure as a 3D platform. Similar finding have been reported in several other studies [56].

4. Conclusion

Wound care and treatment have always been one of the most important aspects of medical science. Synthetic wound dressings, such as hydrogels, are now considered an alternative treatment, and choosing the appropriate compounds for their preparation plays an important role in increasing their efficiency as an ideal wound dressing. Here, we prepared a multi-component hydrogel with enhanced antibacterial efficiency, containing PVA, AgTA NPs, and L. The method of hydrogel fabrication was simple, inexpensive, and safe. The

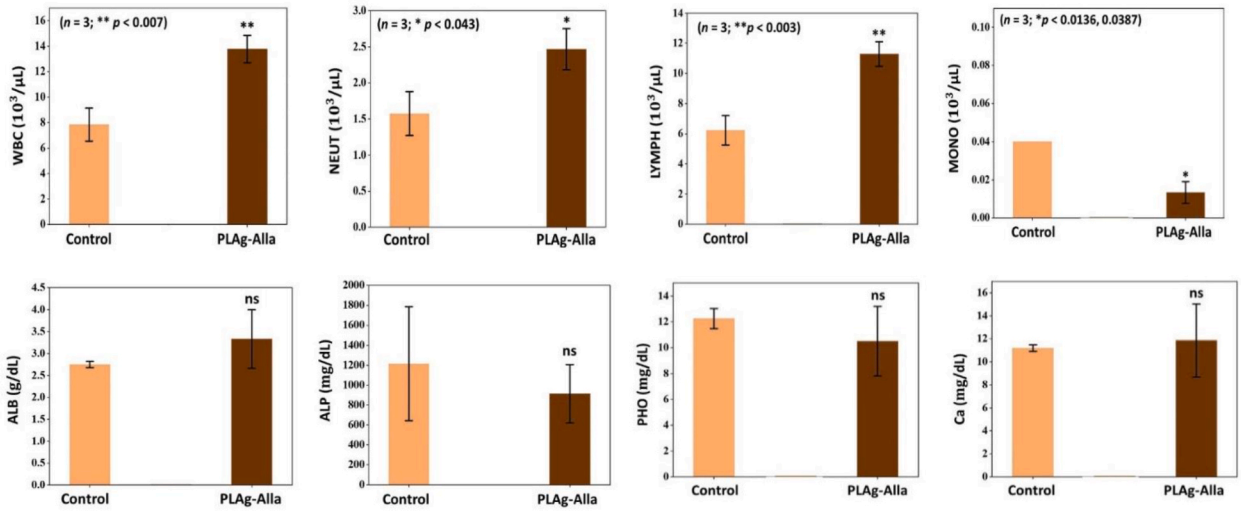

Fig. 10. The hematological and biochemical factors of animals treated with PLAg-Alla hydrogel, (ns; nonsignificant).

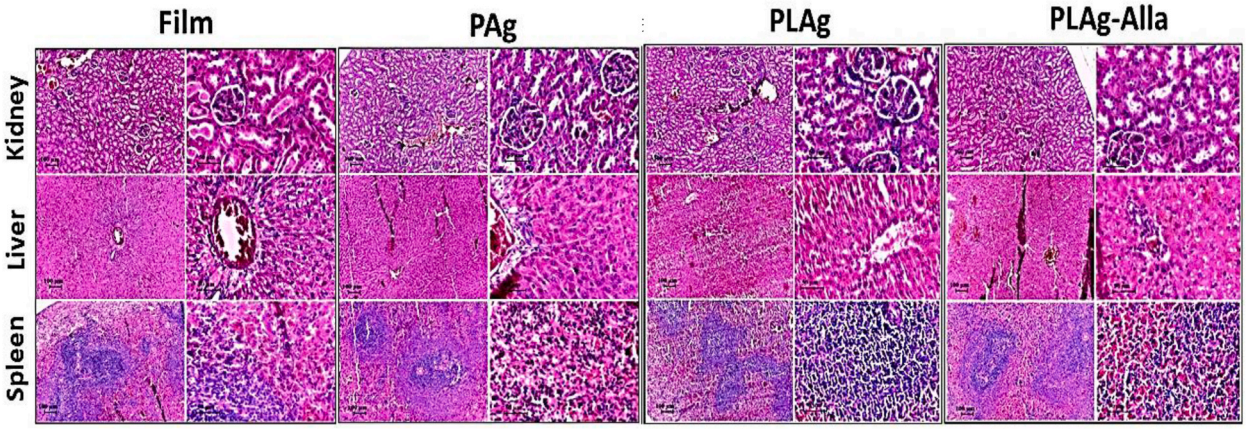

Fig. 11. The H&E staining of kidney, liver, and spleen of treated animal with film, PAg, PLAg, and PLAg-Alla after 14-day of treatment.

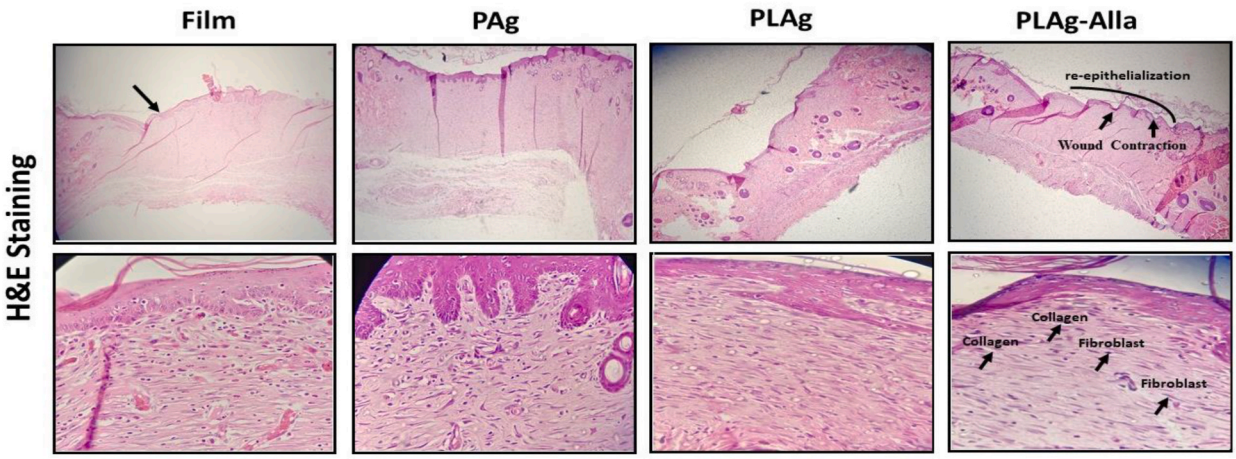

Fig. 12. Histological changes of wound site in animals treated with films, PAg, PLAg and PLAg-Alla hydrogels after 14-day of treatment.

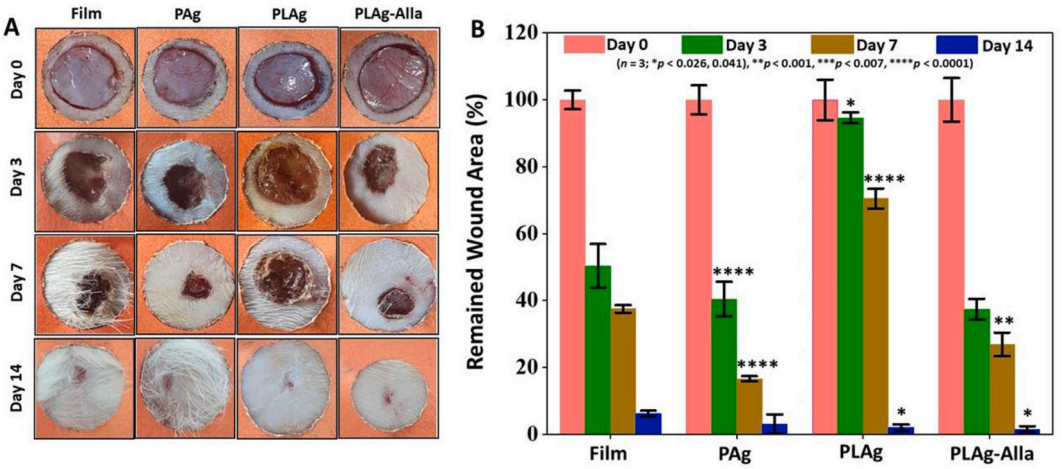

Fig. 13. (A) The Photographs of wound site, (B) the qualification evaluation of wound size during treatment with films, PAg, PLAg and PLAg-Alla hydrogels.

model drug (Alla) was loaded into the hydrogel to reduce inflammation and promote cell proliferation. The physicochemical properties examination confirmed the correct formation of the NPs and hydrogel. The bacterial count test also revealed the excellent antibacterial activity of the hydrogel against two common bacterial strains; *E. coli* and *S. aureus*. Additionally, PLAg-Alla hydrogel materials were biocompatible, physically cross-linked, and stable. Therefore, the prepared hybrid hydrogel can be suggested as a candidate dressing for wounds.

CRediT authorship contribution statement

Fatemeh Hakimi: Writing – original draft, Methodology, Investigation, Conceptualization. **Hadi Balegh:** Writing – review & editing, Validation, Investigation. **Parham Sarmadi fard:** Writing – review & editing, Validation, Software, Investigation. **Fahimeh Kazeminava:** Writing – review & editing, Visualization, Methodology, Investigation. **Sheyda Moradi:** Writing – review & editing, Investigation. **Mehdi Eskandari:** Writing – review & editing, Validation. **Zainab Ahmadian:** Writing – review & editing, Supervision, Resources, Project administration.

Declaration of competing interest

The authors declare that they have no known competing financial interests or personal relationships that could have appeared to influence the work reported in this paper.

References

[1] J. Xiang, L. Shen, Y. Hong, Status and future scope of hydrogels in wound healing: synthesis, materials and evaluation, Eur. Polym. J. 130 (2020) 109609, https://doi.org/10.1016/j.eurpolymj.2020.109609.
[2] N. Mohammad, A. Zainab, M. Zahra, A. Mohsen, Stimuli-responsive systems for wound healing, in: P. Makvandi, E.N. Zare (Eds.), Carrier-mediated Gene and Drug Delivery for Dermal Wound Healing, RSC, 2023, https://doi.org/10.1039/9781837671540-00215.
[3] Z. Ahmadian, M. Ghasemian, F. Hakimi, G. Orive, Cell membrane surface-engineered nanoparticles for dermal wound healing and melanoma (regenerative medicine and cancer therapy of skin). Cell membrane surface-engineered nanoparticles: biomimetic nanomaterials for biomedical applications, in: ACS Symposium Series, American Chemical Society, 2024, pp. 107–149, 1464.
[4] W.J. Caputo, P. Monterosa, D. Beggs, Antibiotic misuse in wound care: can bacterial localization through fluorescence imaging help? Diagnostics 12 (12) (2022) https://doi.org/10.3390/diagnostics12123207.
[5] B. Bullock, M.D. Benham, Bacterial Sepsis. StatPearls. Treasure Island (FL) Ineligible Companies. Disclosure: Michael Benham Declares No Relevant Financial Relationships with Ineligible Companies, StatPearls Publishing Copyright ©, 2024. StatPearls Publishing LLC.; 2024.
[6] H.R.M. Rashdan, M.E. El-Naggar, Chapter 2 - traditional and modern wound dressings—characteristics of ideal wound dressings, in: R. Khan, S. Gowri (Eds.), Antimicrobial Dressings, Academic Press, 2023, pp. 21–42, https://doi.org/10.1016/B978-0-323-95074-9.00002-6.
[7] P. Nezhad-Mokhtari, F. Kazeminava, B. Abdollahi, P. Gholizadeh, A. Heydari, F. Elmi, et al., Matricaria chamomilla essential oil-loaded hybrid electrospun nanofibers based on polycaprolactone/sulfonated chitosan/ZIF-8 nanoparticles for wound healing acceleration, Int. J. Biol. Macromol. 247 (2023) 125718, https://doi.org/10.1016/j.ijbiomac.2023.125718.
[8] F. Kazeminava, S. Javanbakht, M. Nouri, P. Gholizadeh, P. Nezhad-Mokhtari, K. Ganbarov, et al., Gentamicin-loaded chitosan/folic acid-based carbon quantum dots nanocomposite hydrogel films as potential antimicrobial wound dressing, J. Biol. Eng. 16 (1) (2022) 1–13, https://doi.org/10.1186/s13036-022-00318-4.
[9] X. Xue, Y. Hu, S. Wang, X. Chen, Y. Jiang, J. Su, Fabrication of physical and chemical crosslinked hydrogels for bone tissue engineering, Bioact. Mater. 12 (2022) 327–339, https://doi.org/10.1016/j.bioactmat.2021.10.029.
[10] S. Masrour, A. Motavalizadehkakhky, M. Hosseiny, J. Mehrzad, R. Zhiani, F. Kazeminava, Soy protein isolate-based hybrid electrospun nanofibers: an enhanced antimicrobial bio-platform for potential wound healing, J. Polym. Environ. (2023) 1–12, https://doi.org/10.1007/s10924-023-02812-2.
[11] W. Wang, S. Ummartyotin, R. Narain, Advances and challenges on hydrogels for wound dressing, Current Opinion in Biomedical Engineering 26 (2023) 100443, https://doi.org/10.1016/j.cobme.2022.100443.

[12] Y. Wang, M. Zhang, Z. Yan, S. Ji, S. Xiao, J. Gao, Metal nanoparticle hybrid hydrogels: the state-of-the-art of combining hard and soft materials to promote wound healing, Theranostics 14 (4) (2024) 1534–1560, https://doi.org/10.7150/thno.91829.
[13] C. Zhang, K. Liu, Y. He, R. Chang, F. Guan, M. Yao, A multifunctional hydrogel dressing with high tensile and adhesive strength for infected skin wound healing in joint regions, J. Mater. Chem. B 11 (46) (2023) 11135–11149, https://doi.org/10.1039/D3TB01384G.
[14] Y. Zhong, Q. Lin, H. Yu, L. Shao, X. Cui, Q. Pang, et al., Construction Methods and Biomedical Applications of PVA-Based Hydrogels, 12, 2024, https://doi.org/10.3389/fchem.2024.1376799.
[15] S.Y.Z. Moghaddam, E. Biazar, J. Esmaeili, B. Kheilnezhad, F. Goleij, S. Heidari, Tannic acid as a green cross-linker for biomaterial applications, Mini Rev. Med. Chem. 23 (13) (2023) 1320–1340, https://doi.org/10.2174/1389557522666220622112959.
[16] F. Fiori, F.L. Cossu, F. Salis, D. Carboni, L. Stagi, D. De Forni, et al., In vitro antiviral activity of hyperbranched poly-L-lysine modified by L-arginine against different SARS-CoV-2 variants, Nanomaterials 13 (24) (2023), https://doi.org/10.3390/nano13243090.
[17] A. Nicolae-Maranciuc, D. Chicea, L.M. Chicea, Ag nanoparticles for biomedical applications—synthesis and characterization, A Review 23 (10) (2022) 5778, https://doi.org/10.3390/ijms23105778.
[18] F. Kazeminava, S. Javanbakht, M. Nouri, K. Adibkia, K. Ganbarov, M. Yousefi, et al., Electrospun nanofibers based on carboxymethyl cellulose/polyvinyl alcohol as a potential antimicrobial wound dressing, Int. J. Biol. Macromol. 214 (2022) 111–119, https://doi.org/10.1016/j.ijbiomac.2022.05.175.
[19] F. Kazeminava, N. Arsalani, R. Ahmadi, H.S. Kafil, K.E. Geckeler, A facile approach to incorporate silver nanoparticles into solvent-free synthesized PEG-based hydrogels for antibacterial and catalytical applications, Polym. Test. 101 (2021) 106909, https://doi.org/10.1016/j.polymertesting.2020.106909.
[20] F. Kazeminava, S. Javanbakht, M. Zabihi, M. Abbaszadeh, V. Fakhrzadeh, H.S. Kafil, et al., Crosslinking chitosan with silver-sulfur doped graphene quantum dots: an efficient antibacterial nanocomposite hydrogel films, J. Polym. Environ. (2023) 1–12, https://doi.org/10.1007/s10924-023-02929-4.
[21] L. Abdel-Rahman, B. Al-Farhan, D. Abou El-ezz, M. Sayed, M. Zikry, A. Abu-Dief, Green biogenic synthesis of silver nanoparticles using aqueous extract of moringa oleifera: access to a powerful antimicrobial, anticancer, pesticidal and catalytic agents, J. Inorg. Organomet. Polym. Mater. 32 (2022) 1–14, https://doi.org/10.1007/s10904-021-02186-9.
[22] F. Hakimi, M. Sharifyrad, H. Safari, S. Gohari, A.J.H. Ramazani, Amygdalin/chitosan-polyvinyl alcohol/cerium-tannic acid hydrogel as biodegradable long-time implant for cancer recurrence care applications: an in vitro study. https://doi.org/10.1016/j.heliyon.2023.e21835, 2023.
[23] Z. Ahmadian, A. Correia, M. Hasany, P. Figueiredo, F. Dobakhti, M.R. Eskandari, et al., A Hydrogen-bonded Extracellular Matrix-mimicking Bactericidal Hydrogel with Radical Scavenging and Hemostatic Function for pH-responsive Wound Healing Acceleration, 10, 2021 2001122, https://doi.org/10.1002/adhm.202001122, 3.
[24] Z. Ahmadian, H. Gheybi, S. Adeli, Technology, Efficient wound healing by antibacterial property: advances and trends of hydrogels, hydrogel-metal NP composites and photothermal therapy platforms73. https://doi.org/10.1016/j.jddst.2022.103458, 2022.
[25] M. Ghasemian, F. Kazeminava, A. Naseri, S. Mohebzadeh, M. Abbaszadeh, H.S. Kafil, et al., Recent progress in tannic acid based approaches as a natural polyphenolic biomaterial for cancer therapy: a review, Biomed. Pharmacother. 166 (2023) 115328, https://doi.org/10.1016/j.biopha.2023.115328.
[26] X. Yi, J. He, X. Wei, H. Li, X. Liu, F. Cheng, A polyphenol and ε-polylysine functionalized bacterial cellulose/PVA multifunctional hydrogel for wound healing, Int. J. Biol. Macromol. 247 (2023) 125663, https://doi.org/10.1016/j.ijbiomac.2023.125663.
[27] P. Zarrintaj, S. Ghorbani, M. Barani, N.P. Singh Chauhan, M. Khodadadi Yazdi, M.R. Saeb, et al., Polylysine for skin regeneration: a review of recent advances and future perspectives, Bioeng Transl Med 7 (1) (2022) e10261, https://doi.org/10.1002/btm2.10261.
[28] M. Doostmohammadi, S.V. Niknezhad, H. Forootanfar, Y. Ghasemi, E. Jafari, M. Adeli-Sardou, et al., Development of Ag NPs/allantoin loaded PCL/GEL electrospun nanofibers for topical wound treatment, J. Biomater. Appl. 38 (5) (2023) 692–706, https://doi.org/10.1177/08853282231212605.
[29] Z. Ahmadian, A.R. Dargahi, K. Musaie, M.R. Eskandari, Preparation and In Vivo Toxicity Study of Allantoin Incorporated Hyaluronic Acid-L-Cysteine Oral Solution: A Future Treatment for Mucositis</strong&gt, 28, 2022, pp. 414–423, https://doi.org/10.34172/ps.2021.65, 3.
[30] Z. Ahmadian, M. Jelodar, M. Rashidipour, M. Dadkhah, V. Adhami, S. Sefareshi, et al., A self-healable and bioadhesive acacia gum polysaccharide-based injectable hydrogel for wound healing acceleration, Daru :J. Fac. Pharm. 31 (2023), https://doi.org/10.1007/s40199-023-00475-x. Tehran University of Medical Sciences.
[31] Q. Peng, J. Zhu, Y. Yu, L. Hoffman, X. Yang, Hyperbranched lysine-arginine copolymer for gene delivery, J. Biomater. Sci. Polym. Ed. 26 (16) (2015) 1163–1177, https://doi.org/10.1080/09205063.2015.1080482.
[32] I.M. Savic Gajic, I.M. Savic, Z. Svircev, Preparation and characterization of alginate hydrogels with high water-retaining capacity, Polymers 15 (12) (2023), https://doi.org/10.3390/polym15122592.
[33] N. Jaramillo-Quiceno, C. Álvarez-López, G.A. Hincapié-Llanos, C.A. Hincapié, M. Osorio, Characterization of a New Silk Sericin-Based Hydrogel for Water Retention in Soil, 15, 2023, p. 2763, https://doi.org/10.3390/polym15132763, 13.
[34] F. Hakimi, M. Sharifyrad, H. Safari, A. Khanmohammadi, S. Gohari, A. Ramazani, Amygdalin/chitosan-polyvinyl alcohol/cerium-tannic acid hydrogel as biodegradable long-time implant for cancer recurrence care applications: an in vitro study, Heliyon 9 (11) (2023) e21835, https://doi.org/10.1016/j.heliyon.2023.e21835.
[35] F. Hakimi, S. Hashemikia, S.S. Sadighian, A. Ramazani, Nanofibrous chitosan/polyethylene oxide silver/hydroxyapatite/silica composite as a potential biomaterial for local treatment of periodontal disease, Polym. Bull. 80 (2022), https://doi.org/10.1007/s00289-022-04466-x.
[36] C. Bankier, Y. Cheong, S. Mahalingam, M. Edirisinghe, G. Ren, E. Cloutman-Green, et al., A comparison of methods to assess the antimicrobial activity of nanoparticle combinations on bacterial cells, PLoS One 13 (2) (2018) e0192093, https://doi.org/10.1371/journal.pone.0192093.
[37] L. Abdel-Rahman, A. Abu-Dief, R. El-Khatib, S. Mahdy, A. Adam, E.M.M. Ibrahim, Sonochemical synthesis, structural inspection and semiconductor behavior of three new nano sized Cu(II), Co(II) and Ni(II) chelates based on tri-dentate NOO imine ligand as precursors for preparing of metal oxides, Appl. Organomet. Chem. 32 (2017), https://doi.org/10.1002/aoc.4174.
[38] M. Alahmadi, W.H. Alsaedi, W.S. Mohamed, H.M.A. Hassan, M. Ezzeldien, A.M. Abu-Dief, Development of Bi2O3/MoSe2 mixed nanostructures for photocatalytic degradation of methylene blue dye, J. Taibah Univ. Sci. 17 (1) (2023) 2161333, https://doi.org/10.1080/16583655.2022.2161333.
[39] T.T. Bezuneh, N.M. Ofgea, S.S. Tessema, F.A. Bushira, Tannic acid-functionalized silver nanoparticles as colorimetric probe for the simultaneous and sensitive detection of aluminum(III) and fluoride ions, ACS Omega 8 (40) (2023) 37293–37301, https://doi.org/10.1021/acsomega.3c05092.
[40] O. Srichaiyapol, S. Thammawithan, P. Siritongsuk, S. Nasompag, S. Daduang, S. Klaynongsruang, et al., Tannic acid-stabilized silver nanoparticles used in biomedical application as an effective antimelioidosis and prolonged efflux pump inhibitor against melioidosis causative pathogen, Molecules 26 (4) (2021), https://doi.org/10.3390/molecules26041004.
[41] C. Gangwar, B. Yaseen, R. Nayak, S. Praveen, N. Kumar Singh, J. Sarkar, et al., Silver nanoparticles fabricated by tannic acid for their antimicrobial and anticancerous activity, Inorg. Chem. Commun. 141 (2022) 109532, https://doi.org/10.1016/j.inoche.2022.109532.
[42] P.N. Rockwell, J.E. Maneval, B.M. Vogel, E.L. Jablonski, Water diffusion and uptake in injectable ETTMP/PEGDA hydrogels, J. Phys. Chem. B 127 (22) (2023) 5055–5061, https://doi.org/10.1021/acs.jpcb.3c00861.
[43] M.J. Afshari, M. Sabzi, L. Jiang, Y. Behshad, A.R. Zanjanijam, G.R. Mahdavinia, et al., Incorporation of dynamic boronate links and Ag nanoparticles into PVA hydrogels for pH-Regulated and prolonged release of methotrexate, J. Drug Deliv. Sci. Technol. 63 (2021) 102502, https://doi.org/10.1016/j.jddst.2021.102502.
[44] J. Yu, F. Ran, C. Li, Z. Hao, H. He, L. Dai, et al., A lignin silver nanoparticles/polyvinyl alcohol/sodium alginate hybrid hydrogel with potent mechanical properties and antibacterial activity 10 (4) (2024) 240.
[45] S. Song, Z. Liu, M.A. Abubaker, L. Ding, J. Zhang, S. Yang, et al., Antibacterial polyvinyl alcohol/bacterial cellulose/nano-silver hydrogels that effectively promote wound healing, Mater Sci Eng C 126 (2021) 112171, https://doi.org/10.1016/j.msec.2021.112171.
[46] A. Ahsan, M.A. Farooq, Therapeutic potential of green synthesized silver nanoparticles loaded PVA hydrogel patches for wound healing, J. Drug Deliv. Sci. Technol. 54 (2019) 101308, https://doi.org/10.1016/j.jddst.2019.101308.
[47] F. Hakimi, M. Khoshkam, S. Sadighian, A. Ramazani, A facile and high-sensitive bio-sensing of the V617F mutation in JAK2 gene by GSH-CdTe-QDs FRET-based sensor, Heliyon 8 (12) (2022) e12545, https://doi.org/10.1016/j.heliyon.2022.e12545.

[48] H.R. Luthfianti, W.X. Waresindo, D. Edikresnha, A. Chahyadi, T. Suciati, F.A. Noor, et al., Physicochemical characteristics and antibacterial activities of freeze-thawed polyvinyl alcohol/andrographolide hydrogels, ACS Omega 8 (3) (2023) 2915–2930, https://doi.org/10.1021/acsomega.2c05110.
[49] M. Abbas, T. Hussain, M. Arshad, A.R. Ansari, A. Irshad, J. Nisar, et al., Wound healing potential of curcumin cross-linked chitosan/polyvinyl alcohol, Int. J. Biol. Macromol. 140 (2019) 871–876, https://doi.org/10.1016/j.ijbiomac.2019.08.153.
[50] Z. Bai, T. Wang, X. Zheng, Y. Huang, Y. Chen, W. Dan, High strength and bioactivity polyvinyl alcohol/collagen composite hydrogel with tannic acid as cross-linker, Polym. Eng. Sci. 61 (1) (2021) 278–287, https://doi.org/10.1002/pen.25574.
[51] Y. Meng, A sustainable approach to fabricating Ag nanoparticles/PVA hybrid nanofiber and its catalytic activity, Nanomaterials 5 (2015) 1124–1135, https://doi.org/10.3390/nano5021124.
[52] K. Mukherjee, N. Bhagat, M. Kumari, A.R. Choudhury, B. Sarkar, B.D. Ghosh, Insight study on synthesis and antibacterial mechanism of silver nanoparticles prepared from indigenous plant source of Jharkhand, J. Genet. Eng. Biotechnol. 21 (1) (2023) 30, https://doi.org/10.1186/s43141-023-00463-3.
[53] H. Hagh Ranjbar, A. Hosseini-Abari, S.M. Ghasemi, Z. Hafezi Birgani, Antibacterial Activity of Epsilon-Poly-L-Lysine Produced by Stenotrophomonas Maltophilia HS4 and Paenibacillus Polymyxa HS5, Alone and in Combination with Bacteriophages, 169, 2023, https://doi.org/10.1099/mic.0.001363, 7.
[54] W. Ha, J.-L. Yang, Y.-P. Shi, Tannic acid-modified silver nanoparticles for antibacterial and anticancer applications, ACS Appl. Nano Mater. 6 (11) (2023) 9617–9627, https://doi.org/10.1021/acsanm.3c01291.
[55] J. Yu, F. Ran, C. Li, Z. Hao, H. He, L. Dai, et al., A lignin silver nanoparticles/polyvinyl alcohol/sodium alginate hybrid hydrogel with potent mechanical properties and antibacterial activity, Gels (Basel, Switzerland) 10 (4) (2024), https://doi.org/10.3390/gels10040240.
[56] F.M. Aldakheel, D. Mohsen, M.M. El Sayed, K.A. Alawam, A.S. Binshaya, S.A. Alduraywish, Silver nanoparticles loaded on chitosan-g-PVA hydrogel for the wound-healing applications, Molecules 28 (7) (2023), https://doi.org/10.3390/molecules28073241.